Improvement of Traveling Wave-based Fault Location Method for Overhead Distribution Lines

Xinyi Zhang, *Student Member*, *IEEE*, Bingyin Xu, *Member*, *IEEE*,
Zhaoru Han, *Student Member*, *IEEE*, and Fang Shi, *Member*, *IEEE*

***Abstract*—Traveling wave (TW) fault location technology has been widely used in transmission systems due to its high accuracy and simplicity. Recently, there has been growing interest in applying this technology to medium voltage (MV) distribution lines. However, current practices in its deployment, signal measurement, and threshold setting are usually from the application experiences in transmission lines, despite significant differences in fault-induced wave characteristics between transmission and distribution systems. To address these issues, this paper investigates the feasibility and applicability of TW fault technology in MV overhead distribution lines through characteristic analysis of fault-induced TWs. The propagation characteristics of aerial mode and zero mode TWs on overhead distribution lines are studied. Furthermore, it evaluates the influence of critical distribution network components including distribution transformers, multi-branch configurations, and busbar structures on wave propagation characteristics. Deployment strategies for traveling wave fault location (TWFL) devices is proposed to address the unique challenges of distribution networks, while the fault location method is also improved. Field test results demonstrate the effectiveness of the proposed methodology, showing improved fault detection accuracy and system reliability in distribution network applications. This research provides practical implementation suggestions for TWFL technology in distribution networks.**

***Index Terms*—Branch lines, distribution network, overhead lines, propagation characteristics, traveling wave based fault location.**

I. Introduction

Distribution networks directly supply power to users, hence their reliability has a direct impact on customers. Overhead distribution lines are prone to various faults due to the complex surroundings and changing weather conditions. When a fault occurs in the distribution network, efficiently detecting and accurately locating the fault can reduce the time required for manual line patrols and facilitate timely repairs, which is crucial for improving the reliability of power supply [1].

Traditional fault diagnosis methods for distribution lines primarily rely on steady-state power frequency components following a fault occurrence. Their main shortcoming is that they cannot be used to determine the distance of single-phase-to-ground faults in non-solidly grounded (isolated or compensated) systems as the steady-state fault current is very low (only in the range of a few tens amperes). Moreover, these fault location results are significantly influenced by factors such as fault type, distribution network topology, and measurement errors of instrumental transformers. As a result, achieving accurate fault location using power frequency components is challenging.

In contrast, traveling wave fault location (TWFL) methods offer distinct advantages, including high accuracy and simplicity in both principle and implementation. These methods have already proven their effectiveness and have been widely applied in transmission lines [2]–[5]. In addition to their high accuracy (better than 100 m), TW-based methods offer superior reliability by exploiting abundant and prominent transient voltage signals whose magnitudes are comparable to the nominal voltage. Recent advancements in ultra-high-speed data acquisition technology, along with cost reductions, have made the application of TWs for fault location in MV distribution lines a prominent research focus.

A preliminary investigation on the application of TW-based fault location in distribution overhead lines is introduced in [6], in which a novel fault location method is proposed through integrated utilization of initial fault current and voltage traveling wave aerial mode components. A single-end signal expression with fault resistance is deduced in [7], which verifies the applicability of the electromagnetic time reversal method.

Received: February 12, 2025
Accepted: November 5, 2025
Published Online: January 1, 2026
Xinyi Zhang, Zhaoru Han, and Fang Shi are with the School of Electrical Engineering, Shandong University, Jinan 250061, China (e-mail: zhangxy_sdu@163.com; 202234698@mail.sdu.edu.cn; shifang@sdu.edu.cn).

Bingyin Xu (corresponding author) is with the School of Electrical Engineering, Shandong University, Jinan 250061, China; and also with the Kehui Electric. Co., Ltd., Zibo 255049, China (e-mail: xuby@vip.163.com).
DOI: 10.23919/PCMP.2025.000040

However, these two methods lack detailed analysis of the impacts of the heavy ground mode loss, numerous branches and distribution transformers on magnitude and rising time of TW surges. Reference [8] develops a novel fault location algorithm for radial distribution networks, employing synchronized distributed voltage TW observers while quantitatively evaluating transformer impacts on aerial mode wave propagation. A new method using distribution transformers to measure TWs is proposed to solve the problem of obtaining TW signals in feeders' terminal [9]. Nevertheless, the time delay introduced by the voltage transformer to the measured TW signals can reach 2 μs, making it impossible to guarantee fault location errors below 100 m. Therefore, more effective measurement methods need to be explored. The attenuation of zero mode TW propagation in distribution lines and its influence on fault location are investigated in [10], but the rising speed change of zero mode signal is not considered. To remedy this deficiency, the velocity variations of aerial and zero mode TWs are analyzed and a two-terminal fault location method for single-phase grounding faults, based on the time difference of modal TW propagation, is proposed in [11].

The time-frequency wavelet decomposition method proposed in [12] demonstrates enhanced capability in accurately identifying fault characteristic frequencies. Reference [13] employs Shapelet technology to characterize fault features, exhibiting clearer physical interpretability compared to traditional wavelet basis methods. Reference [14] shows that transient signals from different paths have distinct characteristic frequencies forming clusters in energy spectra. Using wavelet-based multi-scale decomposition of voltage signals, the method extracts frequency-band energy distributions to build a neural network diagnostic model. Although wavelet transform offers excellent time-frequency localization properties, its effectiveness is limited by both the dispersion effect during traveling wave propagation and the critical dependence of location accuracy on the proper selection of wavelet bases and decomposition scales.

Reference [15] develops a deep learning method for traveling wave analysis using full-frequency-band components as inputs, achieving accurate wave arrival time detection robust to load switching and operational changes. Additionally, the fault distance can be determined by using the amplitude ratio of different frequency components in the zero mode surge at the measuring point [16]. In [17], a method is proposed for selecting the frequency band that best characterizes the zero mode wavefront by using zero mode wave velocity characteristics for calibrating the arrival time of TWs. Nevertheless, ensuring the reliability and accuracy of fault location methods only using zero mode signal is extremely challenging, as the zero mode loss is significantly higher in distribution overhead lines due to the absence of ground wires. To enhance applicability, the combination of time-space domain and frequency domain analyses are employed to achieve more accurate fault location results for radial distribution networks [18]–[20]. As the above methods do not require the calibration of the arrival time of the TW surge, fault location errors caused by waveform distortion can be avoided. However, they are only applicable to simple network configurations, as the influences of numerous branches and transformers are not considered. In [21], variational mode decomposition is employed to process collected fault signals, and a detection method for corresponding fault induced TW surge is proposed. This method contributes to improving the time tagging accuracy of TW surges, yet it cannot overcome the impacts of propagation attenuations and variable wave velocities. In [22], a fault location scheme is proposed using network topology information and TWs generated by circuit breaker reclosing. However, the scheme depends on reclosing operation, so can only be applied to the location of permanent faults. Reference [23] proposes a traveling-wave data preprocessing method based on the sliding-window median absolute deviation approach. By extracting morphological gradient features from the preprocessed signals, this method achieves preliminary screening of transient disturbances from massive transmission line monitoring data. Reference [24] employs sparsity factors to characterize the differences in time-frequency energy distribution between high-impedance ground faults and normal transient disturbances, thereby establishing a detection criterion that significantly enhances the identification capability for high-impedance faults. A fault location method is proposed for distribution networks based on the time matrix of fault TWs [25]. However, the application of the method to practical systems is challenging as it requires a large amount of historic fault data. With the increasing length of distribution network lines and growing number of branch circuits, the network structure become increasingly complex. While the growing number of monitoring points and higher sampling rates of measurement data provide diversified data sources and massive datasets for fault analysis and localization, the substantial computational requirements have largely confined intelligent algorithm-based fault localization to theoretical and simulation studies. In addition, machine learning models for these applications typically suffer from the small-sample problem characteristic of power system fault scenarios [26].

The tower structure, network configuration, neutral treatment, and voltage level of distribution overhead lines differ significantly from those of transmission lines. Consequently, the propagation and characteristics of fault-induced TWs exhibit notable distinctions. Currently, the deployment, measurement, and utilization of TW signals, as well as the setting of triggering thresholds for fault location devices in MV distribution lines, largely rely on experiences from transmission line applications. This reliance has led to issues such as frequent false triggering, unsatisfactory fault location accuracy, and poor reliability. Therefore, it is imperative to

conduct in-depth studies on the impacts of propagation losses, branches, and distribution transformers on the amplitude and rise speed of TW surges in distribution lines. Such studies will allow accurate quantification of these parameters, and optimize the deployment of TW fault location devices and the utilization of fault-induced TW signals.

This paper investigates the propagation characteristics of fault-induced TWs, taking into account factors such as propagation distance, branch lines, and distribution transformers. By analyzing the amplitude and rising time of fault-induced TW surges, recommendations for the deployment of TW fault location devices and the utilization of fault-induced TW signals are presented. The proposed scheme is validated through multi-scenario simulations and field tests on a typical distribution network.

II. Propagation Characteristics of Traveling Waves in Overhead Distribution Lines

A. Frequency Domain Propagation Characteristics

The propagation characteristics of TWs in distributed parameter lines are typically represented by the propagation coefficient γ, expressed as follows [10]:

$$\gamma = \sqrt{(\mathrm{j}\omega L+R)(\mathrm{j}\omega C+G)} \tag{1}$$

where R, L, C, and G are the distributed parameters per unit length of power line. In fact, R and L exhibit frequency-dependent characteristics, meaning that their values vary significantly at different frequencies. γ can be expressed in complex form [10]:

$$\gamma = \alpha + \mathrm{j}\beta \tag{2}$$

where α is the attenuation coefficient which reflects the amplitude attenuation of the signal per unit length; and β is the phase coefficient which reflects the phase shifting of the signal after traveling one unit length. The expression for the attenuation coefficient α is:

$$\alpha = \mathrm{real}(\gamma) = \sqrt{\frac{1}{2}\left[-\omega^2 LC + RG + \sqrt{\left(\omega^2 L^2+R^2\right)\left(\omega^2 C^2+G^2\right)}\right]} \tag{3}$$

Figure 1 illustrates the variation of the attenuation coefficients with frequency, obtained through digital simulation of a typical overhead distribution line and a typical transmission line using the ATP-EMTP software. The simulations employ the frequency-dependent JMarti model (see Appendix A). The parameters calculated by the internal modules of EMTP software for typical lines hold fundamental or guiding significance for forming transient-based fault location methods [27]. From Fig. 1, it is seen that the attenuation of aerial mode components in both the distribution and transmission lines is relatively small, with negligible difference between the two attenuation coefficients. However, the attenuation of zero mode components in the distribution line is significantly higher than in the transmission line. Specifically, attenuation coefficient in distribution line is 0.079 37 Np/km at 100 kHz, compared to only 0.046 10 Np/km in the transmission line.

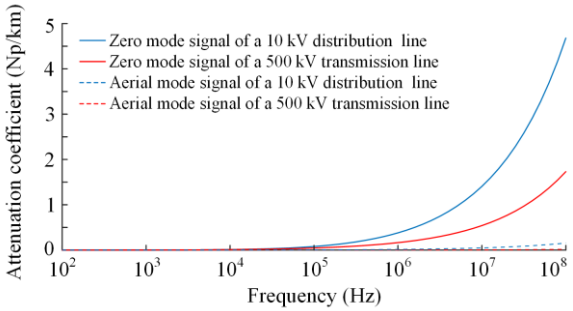

Fig. 1. Attenuation coefficient variation characteristic with frequency.

The high zero mode attenuation in overhead distribution lines is primarily attributed to the absence of lightning protection wires. In these lines, the zero mode TW propagates between the three conductors and the ground, leading to higher attenuation of the high-frequency components of the signal. In contrast, in transmission lines, the zero mode TW propagates mainly between the three conductors and the lightning protection wires, resulting in lower attenuation.

Furthermore, β in (2) can be expressed as follows:

$$\beta = \mathrm{imag}(\gamma) = \sqrt{\frac{1}{2}\left[\omega^2 LC - RG + \sqrt{\left(\omega^2 L^2+R^2\right)\left(\omega^2 C^2+G^2\right)}\right]} \tag{4}$$

Then, the wave velocity can be calculated according to β and the radian frequency of the signal, as:

$$v = \frac{\omega}{\beta} \tag{5}$$

Figure 2 illustrates the increase in velocity of various modal signals in typical lines with frequency. The velocity of all mode signals approaches a maximum value, approximately the speed of light, when the frequency exceeds 50 MHz. The actual frequency components used for TW-based overhead line fault location range from 10 kHz to 500 kHz. In practical field engineering, the wave velocity at 50 kHz, known as the empirical wave speed, is typically used to calculate the distance to a fault [28]. As shown in Fig. 2, the velocity of aerial mode signals for both transmission and distribution lines at 50 kHz is 2.97×10^5 km/s. However, the velocity of zero mode signals increases more slowly with frequency and exhibits much greater variability, particularly for the distribution line, due to higher propagation loss in the ground return path. At 50 kHz, the velocity of zero mode signals is 2.89×10^5 km/s for transmission lines and 2.63×10^5 km/s for distribution lines, both of which are significantly lower than the

empirical wave speed. Therefore, only aerial mode components are considered in transmission line fault location practices to ensure stable and accurate distance-to-fault results.

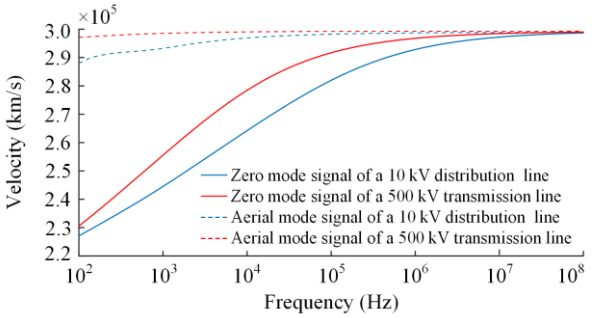

Fig. 2. Wave velocity variation characteristics with frequency.

B. Time Domain Propagation Characteristics

According to fault analysis theory, fault-generated TWs can be studied by introducing a fictitious voltage source. This source has the same amplitude but opposite polarity to the pre-fault voltage. At the moment of fault inception, the voltage of the fictitious source can be considered a DC value. The time-domain propagation characteristics of TWs on power lines can be analyzed by observing the changes in a step signal after it travels a certain distance.

After a step voltage signal travels distance x along the power line, the time-domain expression of the signal is as follows:

$$u(t,x) = F^{-1}\left[U(\omega)\mathrm{e}^{-\gamma x}\right] \tag{6}$$

where F^{-1} is the inverse Fourier transform; and $U(\omega)$ is the frequency domain representation of the step signal.

The corresponding current TW signal is expressed as:

$$i(t,x) = F^{-1}\left[U(\omega)\mathrm{e}^{-\gamma x}/Z(\omega)\right] \tag{7}$$

where $Z(\omega)$ is the wave impedance in frequency domain. The current TW signal exhibits similar propagation characteristics to voltage signals, particularly as the wave impedance approaches a constant value. Therefore, the TW propagation characteristics are studied by analyzing the amplitude and rise time of voltage signals.

Figures 3 and 4 depict the actual voltage waveforms in a typical 10 kV distribution line after a step signal has traveled distances of 1 km, 2 km, 5 km, 10 km, and 20 km, respectively. The rise speeds of zero mode TWs after propagating 1 km, 5 km, and 10 km are measured as 0.85 μs, 6.40 μs, and 14.20 μs, respectively. Comparatively, aerial mode TWs exhibit faster signal transitions with rise times of 0.15 μs, 0.25 μs, and 0.38 μs for the same propagation distances. It can be observed that as the signal travels further, its rising speed decreases, although all waveforms eventually approach the source voltage in their steady state. Specifically, the rising speed of the aerial mode signal is approximately 1 μs after propagating 20 km, whereas the rising speed of the zero mode signal reaches 1 μs after traveling only 2 km.

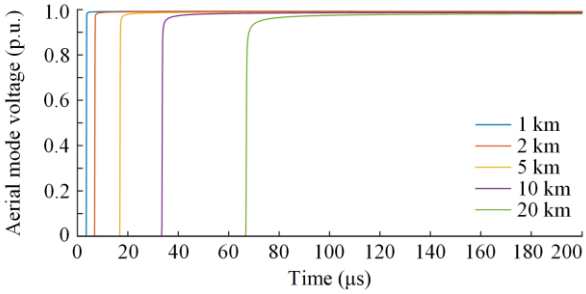

Fig. 3. Propagation characteristics of an aerial mode step signal on the 10 kV overhead line.

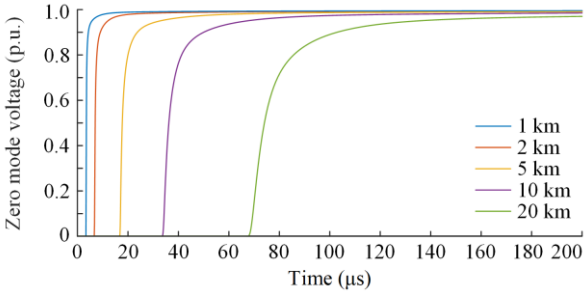

Fig. 4. Propagation characteristics of a zero mode step signal on the 10 kV overhead line.

In contrast, Figs. 5 and 6 illustrate the actual voltage waveforms in the 500 kV transmission line after a step signal has traveled distances of 1 km, 5 km, 10 km, 20 km, and 100 km, respectively. The zero mode TWs demonstrate dispersion characteristics with rise speeds of 0.26 μs, 2.82 μs, and 7.61 μs after propagating 1 km, 5 km, and 10 km, respectively. In contrast, aerial mode TWs exhibit significantly faster transitions, showing merely 0.15 μs, 0.22 μs, and 0.24 μs rise times for the same propagation distances. The rising speeds of the signals differ significantly from those in the distribution line. Specifically, the rising speed of both the aerial mode and zero mode signals reaches approximately 1 μs after traveling 100 km and 3 km, respectively.

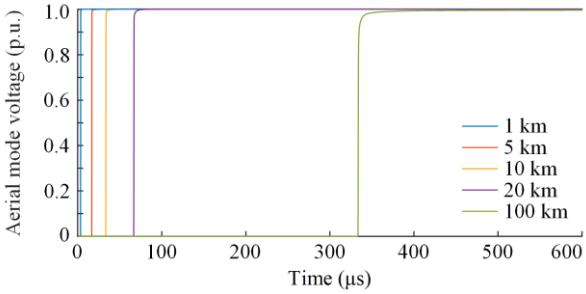

Fig. 5. Propagation characteristics of an aerial mode step signal on the 500 kV overhead line.

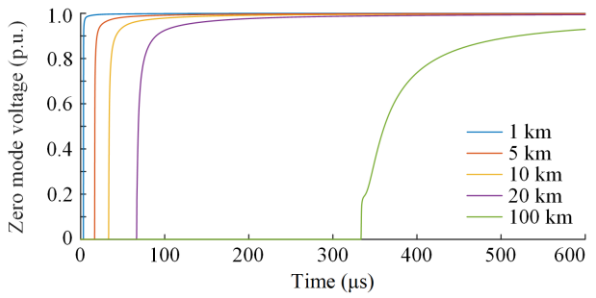

Fig. 6. Propagation characteristics of a zero mode step signal on the 500 kV overhead line.

The threshold for detecting the arrival of TW surges is typically set at 15% of the peak value (0.15 p.u.) generated by a fault, which introduces a detection time delay, as illustrated in Fig. 7. To achieve a distance calculation resolution better than 50 meters, the detection time delay must be less than 0.3 μs. In a simulated typical 10 kV distribution line, after a step signal travels 26 km, the detection delay for aerial mode signals reaches 0.3 μs. In contrast, for zero mode signals, this delay is reached after only 4 km. Consequently, the effective fault location distance is 26 km when using aerial mode signals and 4 km when using zero mode signals.

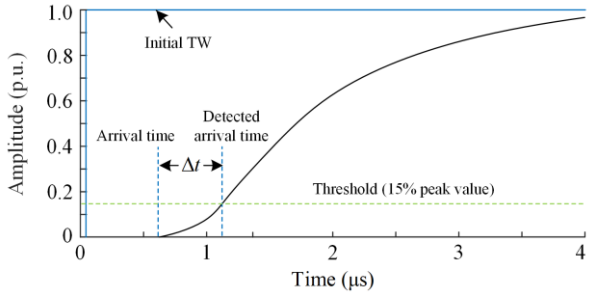

Fig. 7. Arrival time detection of a TW surge.

TW fault location devices in transmission lines typically utilize current TWs. In transmission lines rated at 220 kV and higher, the initial current TW generated by a fault exceeds 400 A, while the rated load current is typically around 2000 A. This significant difference makes it easier to extract fault-generated TW components from the total line currents. In contrast, in 10 kV distribution lines, the rated load current may reach 600 A, but the initial fault-generated current TW is generally no more than 30 A, which is only about 5% of the rated current. To detect faults with a transition resistance greater than 2 kΩ, the triggering threshold for current TWs should be set below 2 A. However, this threshold is only about 0.3% of the rated current, which may lead to frequent false triggers due to load disturbances or other interferences. Zero mode signals, on the other hand, are not influenced by normal load currents, allowing for a lower detection threshold. Based on the above analysis, the effective fault location distance is less than 4 km when using zero mode signals. Therefore, assuming there are no branch lines or transformers in the distribution lines, the distance between two TW fault location devices should not exceed 4 km when relying solely on current TWs.

The maximum value of voltage TWs generated by a fault in a distribution line is equivalent to the line's normal peak voltage. This characteristic can help overcome the limitations of using current TWs. However, conventional voltage transformers (VTs) typically have inferior TW transformation capabilities compared to current transformers (CTs). This makes it challenging to achieve fault location errors below 100 meters when using voltage signals, due to the slow response of the secondary signals of VTs.

C. Optimized Fault Location Methodology

According to the previous analysis, the fitted amplitude attenuation curve per unit length for zero mode signal propagation is shown in Fig. 8.

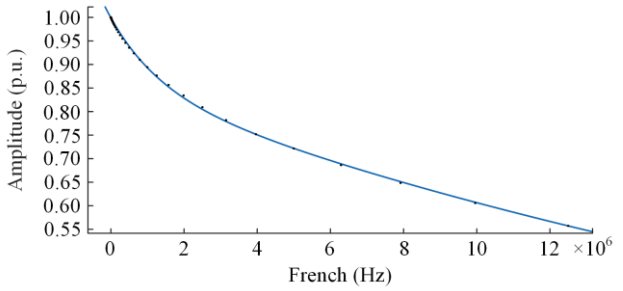

Fig. 8. Fitted curve of the zero-mode signal.

The fitted amplitude formula is given as:

$$A_m(\omega) = 0.08636\mathrm{e}^{-1.598\omega} + 0.8302\mathrm{e}^{-0.07263\omega} \tag{8}$$

When the propagation distance is x km, the wavefront arrival sequence follows the frequency-dependent dispersion characteristics: the highest frequency component arrives first, followed by successively lower frequency components. Consequently, the observed wavefront at the measurement point represents the superposition of all frequency components. Leveraging this physical property, the time-frequency domain propagation function can be decomposed into the superposition of time-domain waveforms corresponding to distinct frequency bands:

$$\begin{aligned} &S(\omega,x)\big|_{\omega=1} = \mathrm{e}^{-\gamma_1 v_1 t_1} \\ &S(\omega,x)\big|_{\omega=1,2} = \mathrm{e}^{-\gamma_1 v_1 t_2} + \mathrm{e}^{-\gamma_2 v_2 t_2} \\ &\quad\vdots \\ &S(\omega,x)\big|_{\omega=1,2,3,\cdots,n} = \mathrm{e}^{-\gamma_1 v_1 t_n} + \mathrm{e}^{-\gamma_2 v_2 t_n} + \mathrm{e}^{-\gamma_3 v_3 t_n} + \cdots + \mathrm{e}^{-\gamma_n v_n t_n} \end{aligned} \tag{9}$$

where $\omega_1, \omega_2, \cdots, \omega_n$ represent distinct frequency components in descending order, and t_n denotes the arrival time of frequency component ω_n at the detection point.

Thus, the time-frequency domain representation of

TW propagation can be derived as:

$$\begin{aligned} &f(t,x)|_1 = A_1 e^{-\gamma_1 v_1 t_1} \\ &f(t,x)|_2 = A_1 e^{-\gamma_1 v_1 t_2} + A_2 e^{-\gamma_2 v_2 t_2} \\ &\vdots \\ &f(t,x)|_n = e^{-(t_n - t_{n-1})} f(t,x)|_{n-1} + A_n e^{-\gamma_n v_n t_n} = \\ &A_1 e^{-\gamma_1 v_1 t_n} + A_2 e^{-\gamma_2 v_2 t_n} + A_3 e^{-\gamma_3 v_3 t_n} + \cdots + A_n e^{-\gamma_n v_n t_n} \end{aligned} \tag{10}$$

where $A_1, A_2, \cdots, A_n$ are the amplitude components of the initial traveling wave corresponding to distinct frequencies (ordered from highest to lowest).

The functional dependence of wave propagation velocity on time and distance can be mathematically expressed as:

$$\frac{t_d}{(t_1 - t_n)x} = \frac{r_{th}}{A_1 e^{-\gamma_1 v_1 t_n} + A_2 e^{-\gamma_2 v_2 t_n} + A_3 e^{-\gamma_3 v_3 t_n} + \cdots + A_n e^{-\gamma_n v_n t_n}} \tag{11}$$

where r_{th} represents the detection threshold of the TW device; and t_d denotes the time delay.

Based on the variation characteristics of TW signals before and after a fault, the accurate fault inception point is determined by performing curve fitting on the pre-fault and post-fault signal segments separately, solving the intersection point of the fitted curves through simultaneous equations, and identifying it as the precise fault origin. This method achieves fault location by accurately marking the zero-crossing point of the fault-induced TW. To address significant waveform attenuation and distortion in TW signals, the methodology employs wavelet decomposition to filter out low-frequency interferences, while utilizing the close-open difference operation (CODO) in mathematical morphology to achieve precise localization of wavefront initiation point.

III. The Impacts of Transformers on Traveling Waves

A. The Impact of a Single Transformer

In MV distribution lines, a transformer connected to low voltage (LV) loads introduces a discontinuity in wave impedance, leading to reflections of incident TWs. When neglecting the influence of load impedance on the secondary side, the equivalent circuit for analyzing the propagation of TWs in transformer windings is depicted Fig. 9 [29]. In this model, C_0 represents the self-capacitance to ground per unit length of the winding, and C_s denotes the longitudinal mutual capacitance per unit length of the winding. According to the TW analysis theory in windings, within the first 5 μs after a voltage wave arrives at the transformer, the fluctuation process within the windings has not developed significantly. Therefore, during this period, the impact of a transformer winding on an incident TW surge can be modeled using an entrance capacitor. The capacitance of this entrance capacitor is expressed as follows [29], [30]:

$$C_e = \sqrt{C_0 C_s} \tag{12}$$

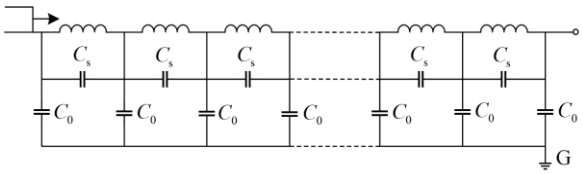

Fig. 9. Distributed parameter circuit model for distribution transformer coil.

According to Petersen's laws of TW theory, the equivalent circuit for calculating the terminal voltage of a transformer when an incident step TW arrives is depicted in Fig. 10. In this circuit, E represents the incident voltage TW, and Z denotes the impedance of line waves.

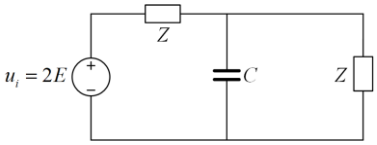

Fig. 10. Transformer's equivalent circuit diagram for TWs.

The transformer's high-frequency response can be approximated by an equivalent capacitance, as illustrated in Fig. 10. The time domain expression of the voltage is:

$$U_m = U\left(1 - e^{-\frac{t}{\tau}}\right) \tag{13}$$

where $\tau = \frac{ZC}{2}$ is the rise time constant.

For typical overhead lines, the aerial mode impedance is approximately 300 Ω, while the zero mode impedance is around 500 Ω. The typical capacitance values for both aerial mode and zero mode are approximately 1000 pF. Therefore, the time constants of the aerial mode and zero mode are approximately 0.15 μs and 0.25 μs, respectively.

The rise times for both the aerial mode and zero mode voltages are 0.60 μs and 1.00 μs, respectively (as shown in Fig. 11). With the threshold at 15% of the peak value (0.15 p.u.), the detection time delays for the aerial mode and zero mode voltages are only 24 ns and 41 ns, respectively. Therefore, the impact of a single transformer on the detection time delay, and consequently on the fault location result, can be considered negligible.

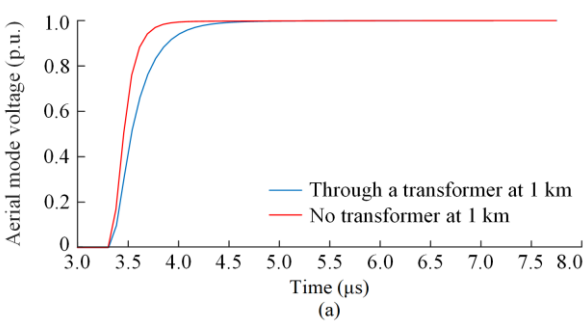

(a)

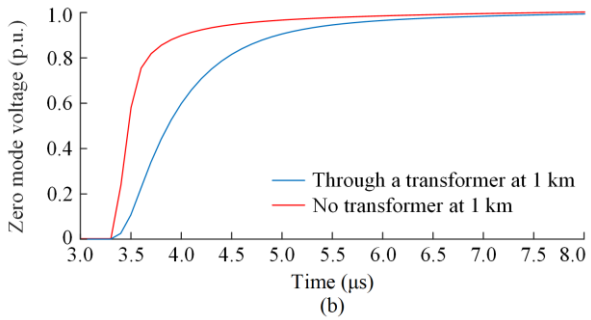

Fig. 11. Impacts of transformers on modal TWs. (a) The aerial mode voltage. (b) The zero mode voltage.

Physical tests on a distribution transformer (see Appendix B for nameplate parameters of the transformer) were conducted to verify the conclusions from the analysis above. The test circuit for observing the transformer's terminal voltage response to an aerial mode incident TW is shown in Fig. 12. In this setup, the lines on both sides of the transformer are simulated using resistors, with resistance equivalent to the magnitude of the aerial mode characteristic impedance.

The incident TW is simulated using a step signal, depicted as the red waveform in Fig. 13, with the voltage response shown as the blue waveform. The ripples observed in the voltage response are due to oscillations caused by the winding inductance, which is typically neglected in theoretical analyses of TWs in transformer windings. The rise times of the incident voltage and the response are 0.2 μs and 0.8 μs respectively. The time delay between two signals is 0.6 μs, which aligns with the conclusions from the analysis above.

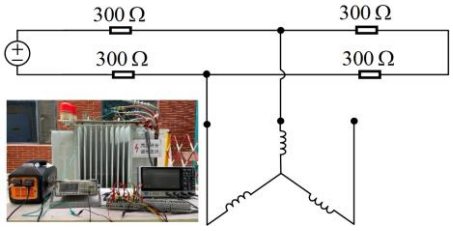

Fig. 12. Test circuit for an aerial mode incident TW.

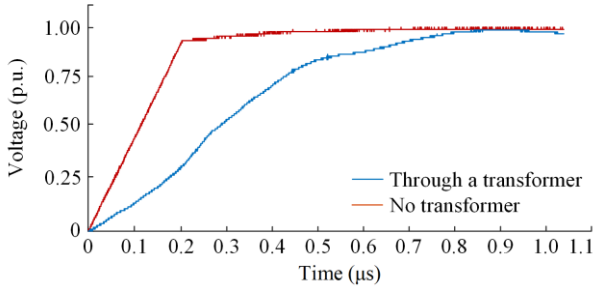

Fig. 13. The voltage response to an aerial mode incident TW.

The voltage response to a zero mode incident TW was tested using the circuit shown in Fig. 14. In this setup, 500 Ω resistors are used to simulate the zero mode wave impedance. The voltage response is depicted as the blue waveform in Fig. 15. As seen, the rise times of the incident voltage and response are 0.2 μs and 1.2 μs. The time delay between the two signals is 1.0 μs, which is also consistent with the theoretical analysis results mentioned above.

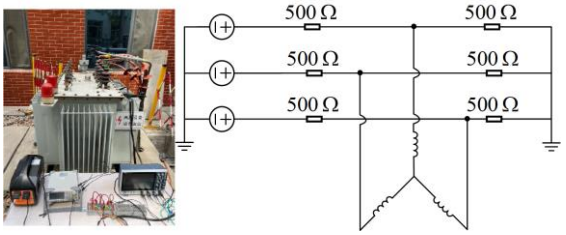

Fig. 14. Test circuit for a zero mode incident TW.

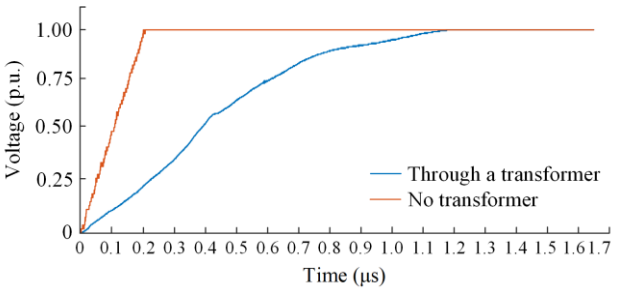

Fig. 15. The voltage response to a zero mode incident TW.

B. The Impacts of Multiple Transformers

There are typically several transformers along distribution lines, as illustrated in Fig. 16. By modeling each transformer with a 1000 pF entrance capacitor and neglecting propagation losses of the lines and subsequent reflections between transformers, the signal waveforms after an aerial mode step voltage passes through 1, 2, 3, and 4 transformers are shown in Fig. 17. With a 0.15 p.u. threshold, the resulting detection time delays are 25 ns, 103 ns, 200 ns, and 307 ns, respectively. It can be concluded that the number of transformers between two TW fault location devices should not exceed 4 when using aerial mode signals, in order to ensure a distance calculation resolution of approximately 50 meters.

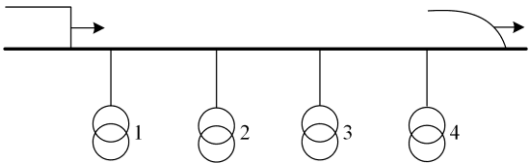

Fig. 16. Transformers on a distribution line.

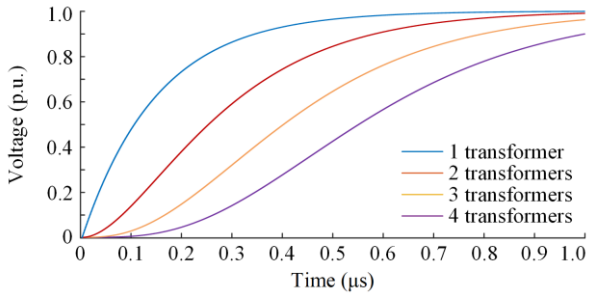

Fig. 17. The impacts of multiple transformers to TWs.

Through similar analysis of the impact of multi-transformers on zero mode TWs, it is found that the number of transformers between two TWFL devices should be more than 3 when using zero mode signals to ensure a distance calculation resolution of approximately 50 meters.

IV. The Impacts of Branches on Traveling Wave Signals

A branch in the distribution line causes attenuation of a TW, which affects the detection delay and the arrival time of the signal.

A. The Attenuation of a Traveling Wave Across a Branch Joint

Figure 18 illustrates the reflected and refracted waves at the junction of a branch, generated by an incident TW u.

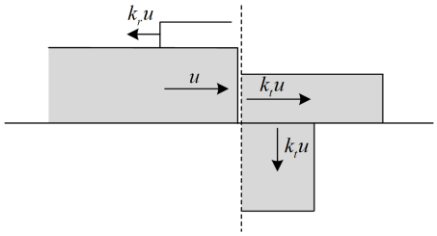

Fig. 18. The reflection and refraction of an incident TW at the joint of branch.

Let Z_1 be the impedance of the main line and Z_2 be the wave impedance of the branch line. The reflected and transmitted waves are, respectively, as follows:

$$u_t = \frac{2(Z_1 // Z_2)}{Z_1 // Z_2 + Z_1} u \tag{14}$$

$$u_r = \frac{Z_1 // Z_2 - Z_1}{Z_1 // Z_2 + Z_1} u \tag{15}$$

Assuming Z_1 is equal to Z_2, the amplitude of the refracted TW is 2/3 of the incident wave, while the reflected wave is −1/3 of the incident wave. The voltage of the line after branch decreases to 67%, indicating that the branch causes 33% attenuation to the TW. Similarly, it can be deduced that the attenuations resulted from 2, 3 and 4 branches are 55.6%, 70.4%, and 90.3%, respectively. This results in the amplitude of the TW decreasing to less than 10% of the fault-generated initial TWs. Therefore, the number of branches between two TW fault location devices should not exceed 2 to ensure reasonable fault detection sensitivity.

B. The Impact of the Length of a Branch

As shown in Fig. 19, the refracted wave entering the branch will reflect back and forth within the branch, causing changes in voltage at the branch point. By neglecting the line loss and the influence of the entrance capacitor of the transformer at the other end of the branch, the voltage at the branch point can be expressed as:

$$U_B = k_t U(t) + k_t^2 U(t+2\tau) + k_t^2 k_r U(t+4\tau) + k_t^2 k_r^2 U(t+6\tau) + \cdots \tag{16}$$

where $U(t)$ is the incident step voltage; and τ is the propagation time of the TW on the branch.

The waveform of the voltage at the branch point rises in a stepwise manner, as shown in Fig. 20. It approaches the amplitude of the incident wave after multiple reflections. If the length of the branch is less than 50 m, the voltage will increase to 1.11 times the incident wave within 0.33 μs, which is beneficial for sensitive detection of TWs. Therefore, the impact of a branch can be neglected when its length is less than 50 m.

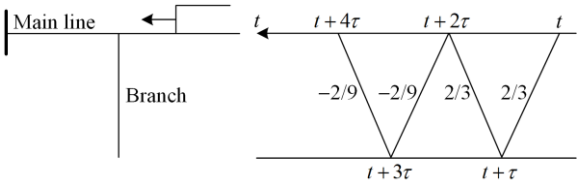

Fig. 19. TW grid diagram for a branch.

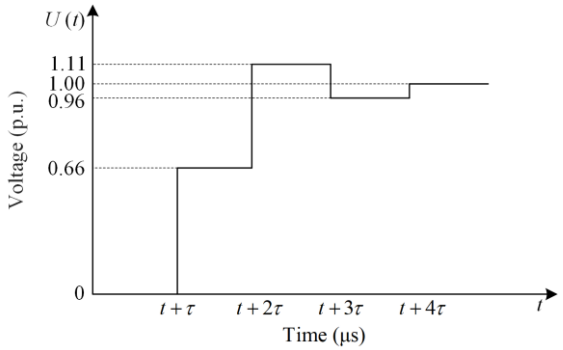

Fig. 20. Voltage at the joint of the branch.

Fault traveling waves are injected 1 km from the branch point, and their propagation is simulated on branch lines of varying lengths. The resulting waveforms at the junction are shown in Fig. 21.

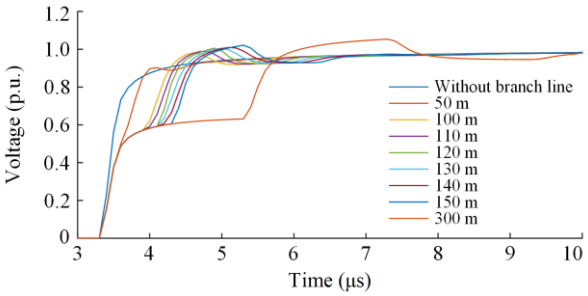

Fig. 21. Effect of branch line length on rise speed.

As shown in Table I, the amplitude reaches 91% of the original value with a rise speed below 1 μs when no branch line is present. With branch line lengths of 130 m, 140 m, 150 m, and 300 m, the amplitudes are attenuated to 74%, 66%, 61%, and 61%, respectively. Under the criterion of rise time below 1 μs, the amplitude increases

to 89% for 100 m branch lines, which proves that branch lines shorter than 100 m have a negligible impact on wavefront steepness. For branch lines exceeding 150 m, the amplitude is reduced by 33%, corresponding to 66% of the original rise speed.

TABLE I
IMPACT OF BRANCH LINE LENGTH ON WAVEFRONT AMPLITUDE GRADIENT (1 μs WINDOW)

Length (m)	0	50	100	110	120	130	140	150	300
Amplitude (%)	91	91	89	87	82	74	66	61	61

V. THE IMPACTS OF BUSES ON TWS

There are usually multiple outgoing feeders in a bus in MV distribution systems. Figure 22 depicts a configuration of a bus with $n+1$ outgoing feeders, where C is the distributed capacitance at the bus.

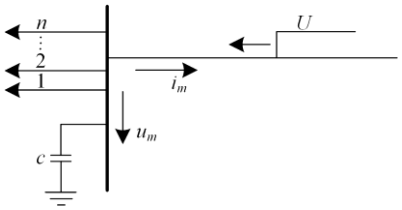

Fig. 22. A bus in a MV distribution system.

The equivalent circuit for calculating the bus voltage and the line current generated by an incident step voltage U is shown in Fig. 23, where Z is the wave impedance of a line. The bus voltage can be expressed as follows:

$$u_m(t)=\frac{2}{1+n}U\left(1-\mathrm{e}^{-\frac{t}{\tau}}\right) \tag{17}$$

where $\tau=\dfrac{ZC}{n+1}$ is a time constant.

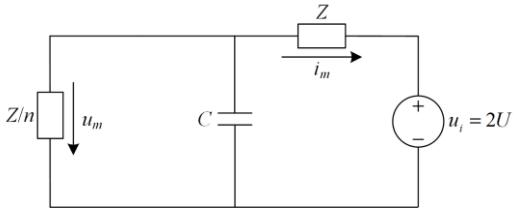

Fig. 23. A bus in a MV distribution system.

It can be seen from (17) that the bus voltage rises exponentially from zero to its maximum value $\dfrac{2}{n+1}U$. The distributed capacitance of the bus is typically more than 2000 pF and the number of other outgoing lines is no less than 5. Assuming the wave impedance of the line is 300 Ω and the threshold for detecting TWs is 0.15 p.u., the detection delay is more than 60 ns representing less than 9 m distance calculation error which is sufficient to ensure fault location accuracy.

Nevertheless, the terminal impedance at a bus is much smaller when there is one or more outgoing cable feeders as the wave impedance of a cable feeder is usually less than 30 Ω. The terminal impedance is less than 15 Ω if there are more than two outgoing cable feeders, and the bus voltage will be less than 10% of the incident voltage. Therefore, the TWFL device may fail to detect the TWs in these cases.

The expression for the current of the line is:

$$i_m(t)=-\frac{2n}{1+n}\frac{U}{Z}\left(1+\frac{1}{n}\mathrm{e}^{-\frac{t}{\tau}}\right)=-\frac{2n}{1+n}\left(1+\frac{1}{n}\mathrm{e}^{-\frac{t}{\tau}}\right)I \tag{18}$$

where $I=\dfrac{U}{Z}$ is the amplitude of the incident current TW.

Equation (18) shows that the initial line current is twice the incident current, which is conducive to detect incoming TWs. However, the amplitude of fault generated current TWs are generally less than 30 A. It is challenging to balance between avoiding frequent triggering of TWFL devices and high TW detection sensitivity when using current signals, as described in Section II.B.

VI. DEPLOYMENT SCHEME AND VERIFICATIONS

A. Deployment Scheme

The TW devices (i.e., TDUs) are usually installed at ends of a line (i.e., substations) in transmission systems. However, due to TW surges have larger attenuation and loss in distribution networks, TDUs need to be installed in the middle of a distribution line for supporting accurate detection of its arriving time, as a fault induced TW surges may not reach the ends of a line with sufficient magnitude. A basic rule of the deployment of TDUs is that for any fault occurring in a distribution overhead line the induced TW surge should be detected reliably with an error of less than 1 μs by at least one TDU in both directions from the fault point. Based on the above analysis of the attenuation and rising time of fault induced TW surges, a TDU deployment scheme in a MV distribution overhead line is proposed as follows.

1) A TDU should be installed with the circuit breaker in the primary substation feeding the line. The current signals, rather than voltage signals, should be used for detecting TW surges as low wave impedance in the bus exits limits the magnitude of voltage signals. In addition, the zero mode current signal is preferable for locating ground faults, particularly for faults occurring within a distance of 4 km.

2) The end of the trunk line and all ends of branches should be equipped with TDUs to locate any faults in the line within less than 100 m error. The TW voltage signals should be used since the current signals are generally very weak at the ends of lines. For cost saving, TDUs may not be installed in the shorter branches whose length is lower than a certain value, say 500 m. However, this would sacrifice the discrimination of the faults in the branch without TDUs.

3) For lines monitored with distribution automation (DA) systems, it is strongly recommended that the TDU

function is integrated with the DA-RTUs, to add an accurate fault location function to the system at a relatively low additional cost. Moreover, both voltage and current signals can be used as DA as RTUs are typically installed along with sectionalizing switches on the lines where significant current and voltage surges will be produced when a fault surge arrives.

4) To ensure reliable detection of TW surges induced by any faults, the total number of branches and transformers between two TDUs installed at both ends of a line section should be not more than 4. This is to guarantee that the incident TW surges have sufficient magnitude and rising time. This rule implies that TDUs shall be installed along lines with a large number of branches and transformers.

B. Simulation

To verify the feasibility of the TW device deployment and signal utilization scheme, a simulation model is established as shown in Fig. 24. This network comprises three overhead lines, with lengths of 9 km, 15 km, and 20 km, respectively. The parameters of the lines and the transformers along the lines are given in Appendices A and B, respectively. TDU1 and TDU3 are installed at the substation exit and the end of line L_1, respectively. TDU2 and TDU4 are installed at both ends of the 3 km long branch. To reduce cost, TDUs are not installed in the three short branches whose lengths are less than 500 m. A single-phase-to-ground fault at phase A occurs at point k2.

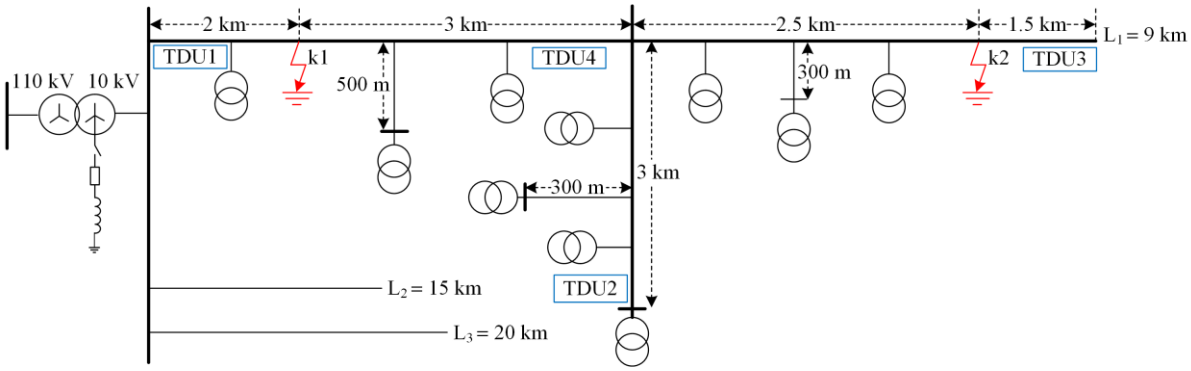

Fig. 24. Simulation model for the deployment scheme of TDUs.

The ATP-EMTP software is used for digital simulation with 0.1 μs time step. The type of signals used, the corresponding threshold and the TW time tag delay of TDU1-TDU4 are given in Table II. Figs. 25 (a) and (b) show the phase current waveforms of the fault TW detected by TDU1 and TDU4, respectively, and Figs. 26 (a) and (b) show the zero mode current waveforms of the fault TW detected by TDU1 and TDU4, respectively. The shortest time tag delays for TDU1 and TDU2 are 2 μs and 1.8 μs, respectively. Therefore, the fault location errors are about 300 m when using time tags of TDU1 and TDU3, and 270 m for TDU2 and TDU3. In comparison, the shortest time tag delay for TDU4 is only 0.8 μs, and the fault location error is about 120 m.

TABLE II
TRIGGER DELAY TIME OF THE FAULT TRAVELING WAVE FOR K2

	Phase current	Zero mode current	Aerial mode voltage	Zero mode voltage
Triggering threshold	5 A	1 A	1000 V	300 V
TDU1	2 μs	2.9 μs	×	2.7 μs
TDU2	×	×	×	1.8 μs
TDU3	×	×	<0.1 μs	<0.1 μs
TDU4	0.9 μs	1.0 μs	2.7 μs	0.8 μs

Note: × represents that the TWFL device cannot be triggered.

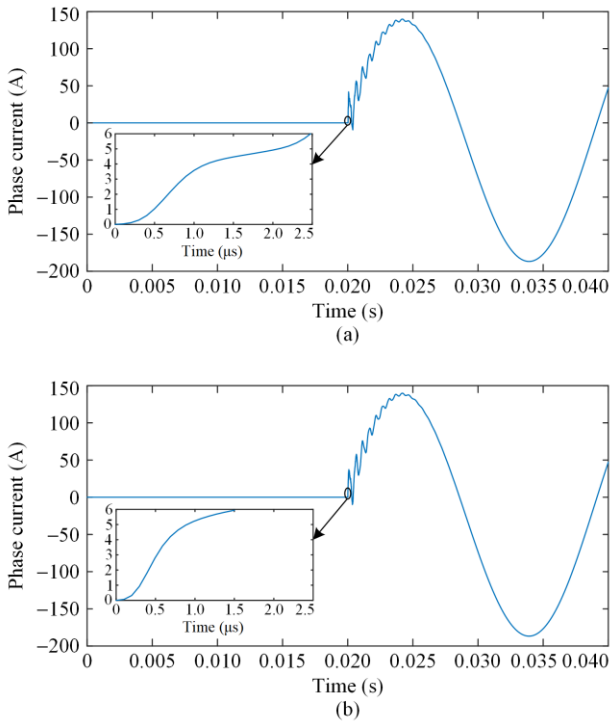

Fig. 25. The phase current waveform of the fault TW. (a) The fault TW detected by TDU1. (b)The fault TW detected by TDU4.

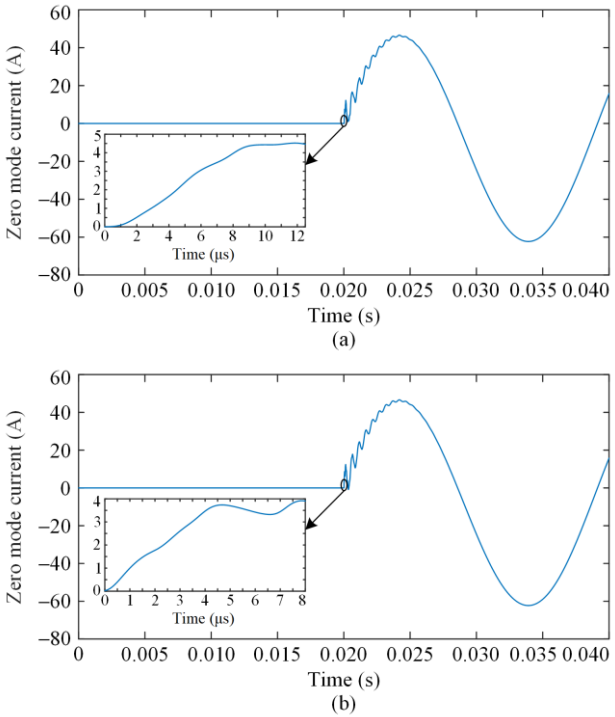

Fig. 26. The zero mode current waveform of the fault TW. (a) The fault TW detected by TDU1. (b) The fault TW detected by TDU4.

Figures 27 (a) and (b) show the zero mode voltage waveforms of the fault TW detected by TDU2 and TDU4, respectively.

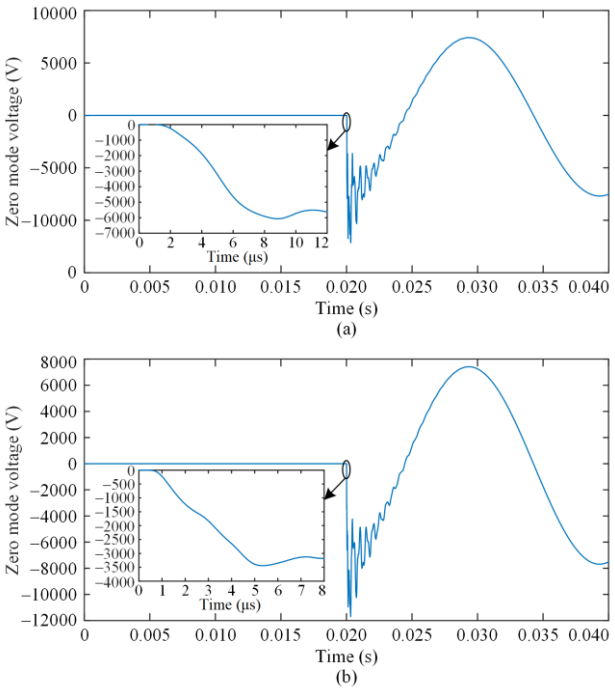

Fig. 27. The zero mode voltage waveform of the fault TW. (a) The fault TW detected by TDU2. (b) The fault TW detected by TDU4.

Similarly, considering a fault at k1, which is 2 km away from the bus, the TW time tag delay for TDU1–TDU4 are presented in Table III. The fault location error is 330 m by TDU1 and TDU3, 270 m by TDU1 and TDU2, and 90 m by TDU1 and TDU4.

TABLE III
TRIGGER DELAY TIME OF THE FAULT TRAVELING WAVE FOR K1

	Phase current	Zero mode current	Aerial mode voltage	Zero mode voltage
Triggering threshold	5 A	1 A	1000 V	300 V
TDU1	0.2 μs	0.3 μs	×	0.6 μs
TDU2	×	×	2.6 μs	1.6 μs
TDU3	×	×	2.6 μs	2.0 μs
TDU4	0.4 μs	0.5 μs	4.0 μs	0.6 μs

Note: × represents that the TWFL device cannot be triggered.

From the above simulation results, it can be seen that by installing TDU4 in the middle of line, a fault location error of less than 150 m can be ensured. The additional installation helps to overcome the long time delay caused by multiple branches and transformers, thereby verifying the correctness of the proposed TDU deployment principles.

C. Field Test

1) Test 1

According to the requirements of the National Key R&D Program "Research on Key Technologies for Smart Distribution Network Operation Based on Micro Synchronized Phasor Measurement," an embeddable fault location unit compatible with PMU devices is under development. This integrated unit will share measurement signal channels, synchronization clocks, power modules, and communication interfaces with host PMUs to achieve cost reduction and facilitate large-scale deployment.

In a practical implementation case, 14 PMU devices have been installed on a 10 kV feeder line in a 35 kV substation with arc suppression coil grounding system located in China's coastal region. Among these, 6 PMUs are equipped with integrated TWFL units (specific installation locations are shown in Fig. 28). All device data is aggregated into the distribution automation master station, enabling comprehensive fault diagnosis and precise localization through the synergistic use of synchronized phasor measurements from PMUs and traveling wave detection data from TWFL units.

To comprehensively validate the functionality and performance of the proposed fault diagnosis and localization method, a controlled manual grounding fault test was implemented at pole 4123 A on the distribution line. A grounding ring was installed on phase C of the overhead line segment, and a fixed downlead cross-arm is mounted below the straight cross-arm on the pole. The grounding fault test is completed using an electrical operation switch. The developed software module is tested through on-site witnessed trials, with the primary

objective of verifying the fault diagnosis and localization functionality as well as the fault location error metrics in the demonstration project. For this test, a distribution line with arc suppression coil grounding was selected, and the test is carried out by artificially triggering a grounding fault. A total of three test cases are conducted. The evaluation criteria are: 1) For each fault, the system must correctly identify the faulted phase and locate the fault section; 2) The TWFL module must trigger and provide a fault distance measurement with an error of less than 150 m; 3) The system successfully detects all three fault tests, accurately identifies the faulted sections, and provides distance measurements.

A detailed condition is provided below.

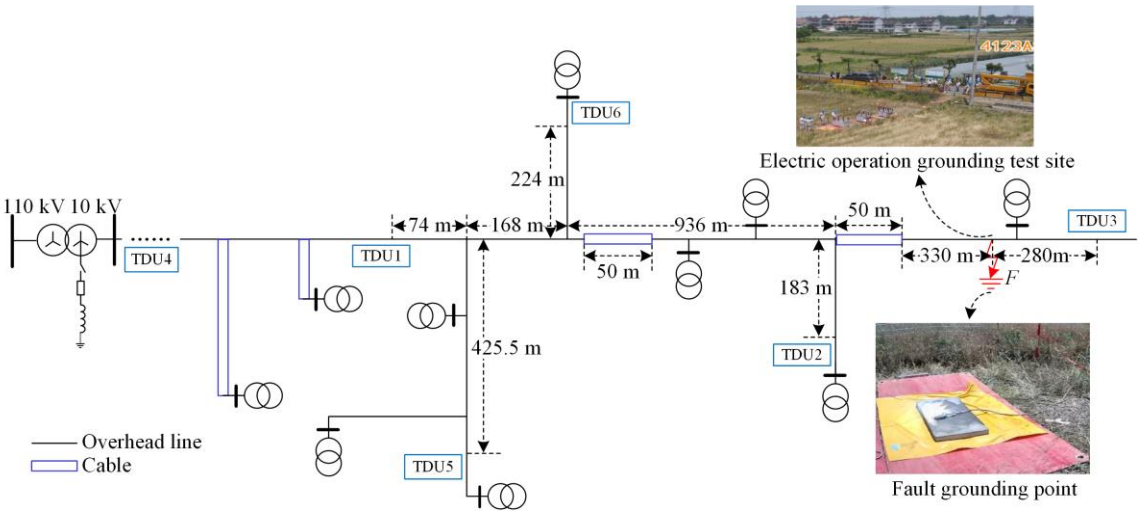

Fig. 28. The installation locations and distances of the fault location devices.

Figure 29 represents the TW arrival time for the first solid grounding fault on phase C.

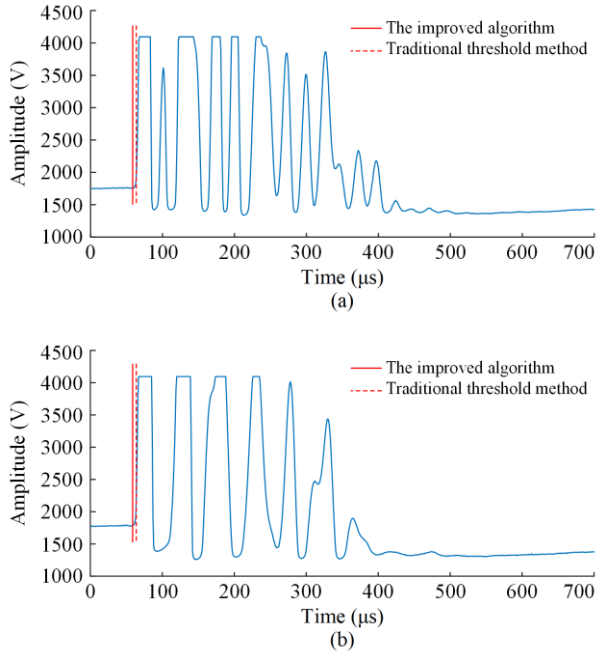

Fig. 29. The first fault location result. (a) TDU3 measured waveform. (b) TDU2 measured waveform

The TWFL improved algorithm determines the initial fault location with the following results: 204 m from TDU3, 639 m from TDU2, and the measured fault location error is 76 m.

Figure 30 gives the TW arrival time for the second solid grounding fault on phase C.

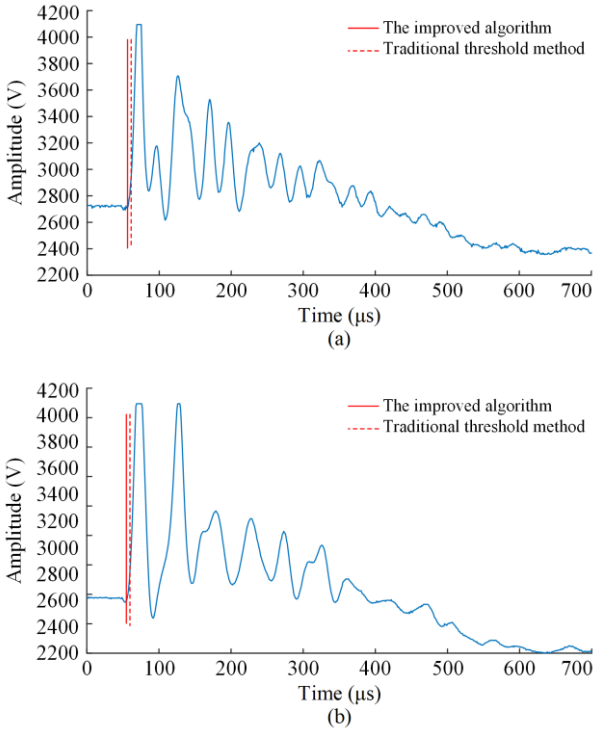

Fig. 30. The second fault location result. (a) TDU3 measured waveform. (b) TDU2 measured waveform

The fault location results indicate: 159 m from TDU3, 684 m from TDU2, with a measurement error of 121 m.

Figure 31 shows the TW arrival time for the phase C

high impedance grounding fault on a concrete surface (with a measured transition resistance of 1580 obtained on-site using a megohmmeter).

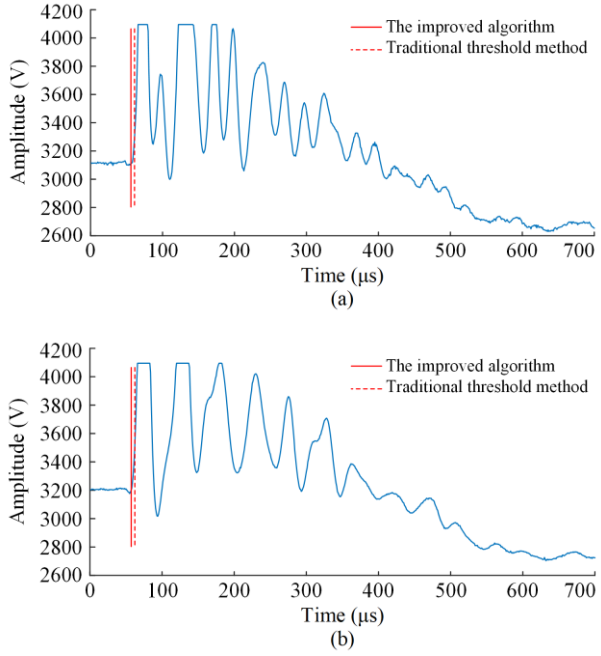

Fig. 31. The third fault location result. (a) TDU3 measured waveform. (b) TDU2 measured waveform

Fault location results: 157 m from TDU3, 686 m from TDU2, positioning error 123 m.

The fault occurred between TDU2 and TDU3. Given that the cable section is shorter than 50 m, its impact on the overhead line can be neglected (the analytical method follows the same principle as for short branch lines), allowing this to be treated as a pure overhead line segment. The fault propagation path passes through one transformer when traveling toward TDU3, and encounters one long branch line when propagating toward TDU2. The time delay caused by this configuration remains within the permissible range of fault location accuracy. The error in practical fault location measurements is primarily caused by sampling rate and time synchronization error, while variations in errors across different tests are also related to the fault resistance present during each incident.

2) Test 2

The accuracy of the proposed fault location algorithm is verified using actual waveform data from a 10 kV test field. As shown in Fig. 32, the distribution system features a hybrid topology comprising four cable lines (Lines 1−4) and one double-circuit overhead line on the same tower (Lines 5−6). During testing, Line 6 is connected to the bus by closing its switch, while a 20 m cable was used to series-connect Line 2 and Line 5. TW measurement devices with 2 MHz sampling rate are installed at key nodes of the overhead line. Through artificial grounding tests simulating various fault conditions (including neutral grounding mode variations and transition resistance adjustments), 42 sets of valid faults traveling wave data are acquired.

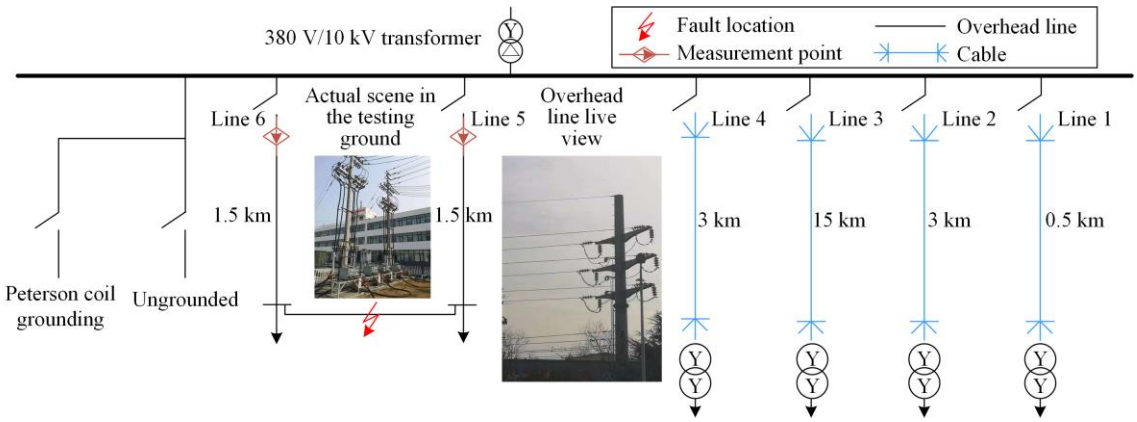

Fig. 32. The topology of 10 kV real test site.

The location results presented in Fig. 33 demonstrate that all test cases achieve measurement errors within 140 m, fully complying with the precision requirements for TWFL.

Figures 34 and 35 present the analysis results of the fault-phase current TWs under a solid grounding fault, processed using wavelet transform and mathematical morphology. The results demonstrate that the CODO variation-based detection method can sensitively and reliably identify the arrival time of the fault-induced TWs.

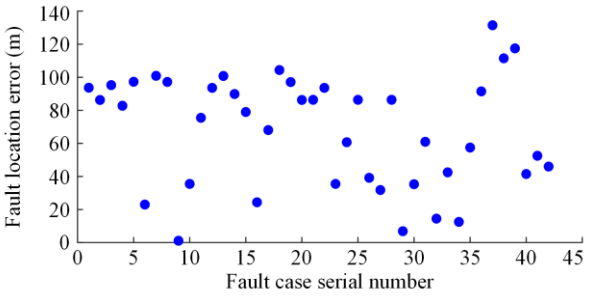

Fig. 33. The results of fault location.

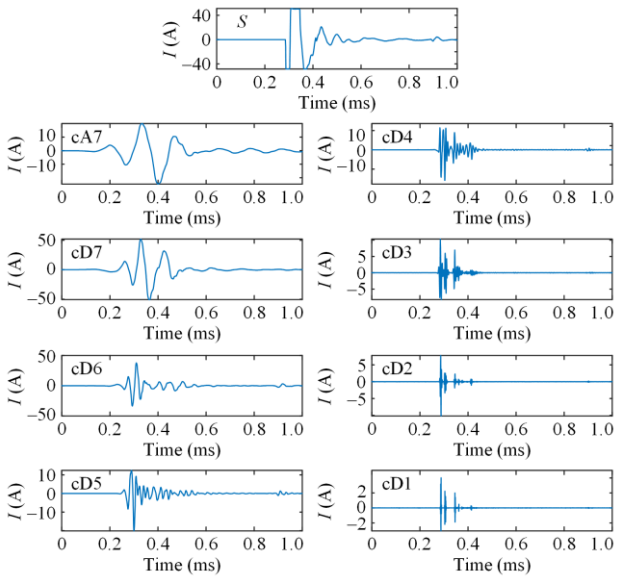

Fig. 34. Wavelet transform example of the test data.

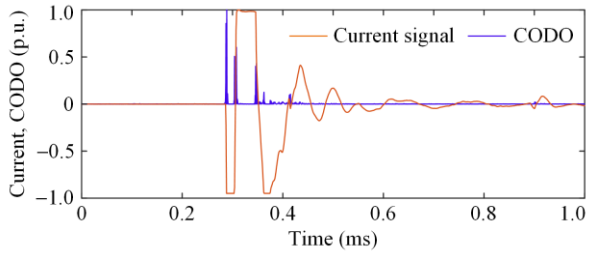

Fig. 35. The time detection of the test data.

VII. Conclusion

This paper studies the applicability and feasibility of TWFL in MV distribution lines by analyzing the propagation characteristics of TWs on overhead distribution lines. The conclusions of the analysis are summarized as follows.

1) Current TWs generated by faults in distribution networks are much smaller compared to the rated load current. It is thus difficult to balance between ensuring higher fault detection sensitivity and avoiding frequent false triggering when using aerial mode current TWs. The effective fault location distance is less than 4 km when using zero mode current TWs due to heavy propagation losses in overhead distribution lines.

2) Branches in distribution lines will result in one third attenuation to the amplitude of TWs. The number of branches between two TWFL devices shall be no more than 4 to ensure an adequate fault detection sensitivity. Nevertheless, a branch lines shorter than 50 m do not have substantial influence on the propagation of TWs, and its impacts on TWFL can be neglected.

3) Distributed capacitances in distribution transformers slow the rise of TWs. Accurate fault location becomes challenging if there are more than 4 transformers between two TWFL devices owing to significant TW rise time delays.

4) At substation buses, voltages produced by the arrival of TWs are usually very weak which can result in fault detection failure. It is also challenging to achieve high detection sensitivity for fault location using current signal. Therefore, further investigations for detecting TWs arriving at buses are needed.

The applicability of TWFL to overhead distribution lines is greatly compromised due to the effects of very low fault current TWs, higher propagation loss, outgoing cable feeders at buses, and the presence of multiple branches and transformers. The voltage signals are preferred for detecting TWs, and the numbers of discontinuity points (such as branches, transformers) between two TWFL devices shall be no more than 4. When discontinuity points exceed 4, accurate fault location can be achieved through combined pre-fault/post-fault signal segment curve fitting analysis and an integrated wavelet-morphology processing methodology.

Appendix A

The structures of the 10 kV and 500 kV lines used for the simulation are shown in Fig. A1 and Fig. A2, respectively. The parameters for the 10 kV line are as follows: the wire type is specified as JKLYJ-185, with a unit length resistance of 0.2422 Ω/km and a soil resistivity of 100 Ω·m. The parameters for the 500 kV line are as follows: the wire specification is LGJQ-300*4, with a 4-split configuration and a phase spacing of 0.45 meters. The direct current resistance is 0.108 Ω/km for the wire and 0.374 Ω/km for the ground wire. The soil resistivity is recorded at 100 Ωm .

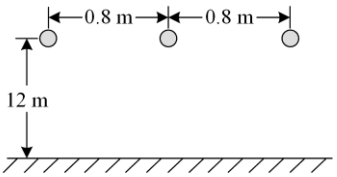

Fig. A1. A 10 kV typical overhead distribution line's tower structure model.

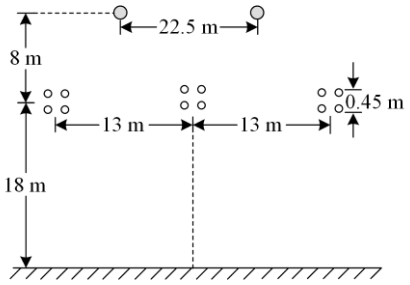

Fig. A2. A 500 kV typical overhead transmission line's tower structure model.

APPENDIX B

The nameplate parameters of the tested transformer are listed in Table BI.

TABLE BI
PARAMETERS OF THE TESTED TRANSFORMER

Parameter	Value
Rated capacity	800 kVA
Rated voltage	10 kV±5%/400 V
Connection mode	Yyn
Short-circuit impedance	4.65%

ACKNOWLEDGMENT

Not applicable.

AUTHORS' CONTRIBUTIONS

Xinyi Zhang: writing original draft, software, methodology, formal analysis and conceptualization. Bingyin Xu: resources, supervision, writing review, editing, and validation. Zhaoru Han: writing review, editing, data curation and visualization. Fang Shi: resources, supervision, writing review, editing, and data curation. All authors read and approved the final manuscript.

FUNDING

This work is supported by the National Natural Science Foundation of China (No. 52107109).

AVAILABILITY OF DATA AND MATERIALS

Not applicable.

DECLARATIONS

Competing interests: The authors declare that they have no known competing financial interests or personal relationships that could have appeared to influence the work reported in this article.

AUTHORS' INFORMATION

Xinyi Zhang received the B.S. degree from North China Electric Power University, Beijing, in 2015, and received the M.S. degree from Qingdao University, in 2018. He is currently pursuing the Ph.D. degree at the Key Laboratory of Power System Intelligent Dispatch and Control of the Ministry of Education, Shandong University, Jinan, China. His research interests include fault diagnosis and location in the distribution system.

Bingyin Xu received the B.S. and M.S. degrees in electrical power engineering from Shandong University, Jinan, China, in 1982 and 1987, respectively, and the Ph.D. degree from Xi'an Jiaotong University, Xi'an, China, and the City University of London, London, UK. in 1991. He is a professor with Shandong University, Jinan, China. His research interests include automation of distribution networks, traveling-wave-based fault location, and the application of IEC 61850 in distribution systems.

Zhaoru Han received the B.S. degree in Electrical Engineering from Taiyuan University of Technology, Taiyuan, China, in 2022. He is currently pursuing the Ph.D. degree at the Key Laboratory of Power System Intelligent Dispatch and Control of the Ministry of Education, Shandong University, Jinan, China. His research interests include fault diagnosis and location in the distribution system.

Fang Shi received the B.S. degree in electrical engineering from the China University of Petroleum, Dongying, China in 2006, and received the M.S. degree in electrical engineering from the State Grid Electric Power Research Institute, Nanjing, China in 2009, and the Ph.D. degree from Shanghai Jiao Tong University, Shanghai, China in 2014. He is currently an associate professor in the Key Laboratory of Power System Intelligent Dispatch and Control of the Ministry of Education, Shandong University, Jinan, China. His research interests include power system stability and control and phasor measurement units (PMU) technology and its applications.

REFERENCES

[1] X. Wang, H. Zhang, and F. Shi *et al*., "Location of single phase to ground faults in distribution networks based on synchronous transients energy analysis," *IEEE Transactions on Smart Grid*, vol. 11, no. 1, pp. 774-785, Jan. 2020.

[2] Y. Xia, Z. Li, and Y. Xi *et al*., "Accurate fault location method for multiple faults in transmission networks using travelling waves," *IEEE Transactions on Industrial Informatics*, vol. 20, no. 6, pp.8717-8728, Jun. 2024.

[3] F. Deng, X. Zeng, and L. Pan, "Research on multi-terminal traveling wave fault location method in complicated networks based on cloud computing platform," *Protection and Control of Modern Power Systems*, vol. 2, no. 2, pp. 1-12, Apr. 2017.

[4] J. C. Quispe, J. Morales, and E. Orduna *et al*., "Time-frequency multiresolution of fault-generated transient signals in transmission lines using a morphological filter," *Protection and Control of Modern Power Systems*, vol. 8, no. 2, pp. 1-14, Apr. 2023.

[5] J. Luo, Y. Liu, and Q. Cui *et al*., "Single-ended time domain fault location based on transient signal measurements of transmission lines," *Protection and Control of Modern Power Systems,* vol. 9, no. 2, pp. 61-74, Apr. 2024.

[6] T. Ji, Y. Xue, and T. Sun *et al*., "Fault location for distribution feeders based on traveling waves," *Automation of Electric Power Systems*, vol. 29, no. 19, pp. 66-71, Oct. 2005. (in Chinese)

[7] H. Cui, Q. Yang, and J. Sun *et al*., "Electromagnetic time reversal fault location method based on characteristic frequency of traveling waves," *IEEE Transactions on Power Delivery*, vol. 38, no. 5, pp. 3033-3044, Oct. 2023.

[8] A. Tashakkori, P. J. Wolfs, and S. Islam *et al*., "Fault location on radial distribution networks via distributed synchronized traveling wave detectors," *IEEE Transactions on Power Delivery*, vol. 35, no. 3, pp. 1553-1562, Jun. 2020.

[9] T. Ji, T. Sun, and B. Xu *et al*., "Traveling waves measurement with distribution transformers," *Automation of Electric Power Systems*, vol. 30, no. 16, pp. 66-71, Aug. 2006. (in Chinese)

[10] J. Wang, X. Dong and S. Shi, "Traveling wave transmission research for overhead lines of radial distribution power systems considering frequency characteristics," *Proceedings of the CSEE*, vol.33, no. 22, pp. 96-102, Nov. 2013. (in Chinese)

[11] J. Tang, X. Yin, and Z. Zhang *et al*., "Iterative extraction of detected zero-mode wave velocity and its application in single phase-to-ground fault location in distribution networks," *Transactions of China Electrotechnical Society*, vol. 28, no. 4, pp. 202-211, Feb. 2013. (in Chinese)

[12] A. Borghetti, M. Bosetti, and A. C. Nucci *et al*., "Integrated use of time-frequency wavelet decompositions for fault location in distribution networks: theory and experimental validation," *IEEE Transactions on Power Delivery*, vol. 25, no. 4, pp. 3139-3146, Aug. 2010.

[13] S. Pati, M. Biswal, and J. S. Ranade *et al*., "Evaluating the use of shapelets in traveling wave based fault detection and classification in distribution systems," *IEEE Transactions on Industry Applications*, vol. 60, no. 2, pp. 2507-2516, Apr. 2024.

[14] M. Pourahmadi-Nakhli and A. Safavi A, "Path characteristic frequency-based fault locating in radial distribution systems using wavelets and neural networks," *IEEE Transactions on Power Delivery*, vol. 26, no. 2, pp. 772-781, Apr. 2011.

[15] Y. Wang, X. Zeng, and F. Liu *et al.*, "Fault traveling wave head calibration method for a distribution network based on the full band characteristics of a traveling wave," *Power System Protection and Control*, vol. 53, no. 1, pp. 171-80, Jan. 2025. (in Chinese)

[16] M. Xu, L. Xiao, and L. Lin, "A fault location method for the single-phase-to-earth fault in distribution system based on the attenuation characteristic of zero-mode traveling wave," *Transactions of China Electrotechnical Society*, vol. 30, no. 14, pp. 397-404, Jul. 2015. (in Chinese)

[17] Y. Ning, D. Wang, and X. Jiang *et al*., "A single phase-to-ground fault location scheme for distribution networks based on zero-mode traveling wave velocity property," *Proceedings of the CSEE*, vol. 35, no. S1, pp. 93-98, Jan. 2015. (in Chinese)

[18] R. Liang, Z. Jin, and C. Wang *et al*., "Research of fault location in distribution networks based on integration of traveling wave time and frequency analysis," *Proceedings of the CSEE*, vol. 33, no. 28, pp. 130-136, Oct. 2013. (in Chinese)

[19] J. C. Quispe, J. Morales, E. Orduna *et al*., "Time-frequency multiresolution of fault-generated transient signals in transmission lines using a morphological filter," *Protection and Control of Mododern Power Systems*, vol. 8, no. 1, pp. 14-22, Jan. 2023.

[20] H. Shu, X. Liu, and X. Tian, "Single-ended fault location for hybrid feeders based on characteristic distribution of traveling wave along a line," *IEEE Transactions on Power Delivery*, vol. 36, no. 1, pp. 339-350, Feb. 2021.

[21] L. Xie, L. Luo, and Y. Li *et al*., "A traveling wave-based fault location method employing VMD-TEO for distribution network," *IEEE Transactions on Power Delivery*, vol. 35, no. 4, pp. 1987-1998, Aug. 2020.

[22] S. Shi, B. Zhu, and A. Lei *et al*., "Fault location for radial distribution network via topology and reclosure-generating traveling waves," *IEEE Transactions on Smart Grid*, vol. 10, no. 6, pp. 6404-6413, Nov. 2019.

[23] P. Cao, Z. Shen, and H. Shu *et al*., "Identification of lightning interference waveforms in massive traveling wave data based on waveform mutation characteristics," *Automation of Electric Power Systems*, vol. 47, no. 17, pp. 178-186, Sept. 2023. (in Chinese)

[24] F. Deng, F. Xu, and S. Feng *et al*., " Research on high impedance fault detection method based on energy distribution characteristics of traveling wave full waveform," *Proceedings of the CSEE*, vol. 42, no. 22, pp. 8177-8189, Nov. 2022. (in Chinese)

[25] L. Cheng, T. Wang, and Y. Wang, "A novel fault location method for distribution networks with distributed generations based on the time matrix of traveling-waves," *Protection and Control of Modern Power Systems*, vol. 7, no. 44pp. 1-11, Oct. 2022.

[26] J. He, G. Luo, and M. Cheng *et al*., " A research review on application of artificial intelligence in power system fault analysis and location," *Proceedings of the CSEE*, vol. 40, no. 17, pp. 5506-5015, Sept. 2020. (in Chinese)

[27] J. Duan, B. Zhang, and J. Ren *et al*.," Single-ended transient-based protection for EHV transmission lines basic theory," *Proceedings of the CSEE*, vol. 27, no. 1, pp. 37-43, Jan. 2007.

[28] X. Dong, B. Chen, and Q. Dong *et al*., "Traveling waves fault location of distribution lines based on distributed voltage sensing technology," *Power System Technology*, vol. 47, no. 12, pp. 4837-4846, Dec. 2023. (in Chinese)

[29] G. Xie, "The process of traveling wave propagation in windings," in *Overvoltage in Power System*, *2*nd ed., Beijing, China: China Electric Power Press, pp. 103-114, 2018.

[30] E. Dick and C. Erven, "Transformer diagnostic testing by frequency response analysis," *IEEE Transactions on Power Apparatus and Systems*, vol. PAS-97, no. 6 pp. 2144-2153, Nov. 1978.